

Simulations of a Complex Robotic System

Satish S. Nair
 Dept. of Mechanical Engineering
 Wayne State University
 Detroit, Michigan

ABSTRACT

Dynamic simulations of a six-legged rough terrain walking machine power and leg actuation and control systems are presented. Digital simulation was found to be essential, in addition to analytical modeling, for characterizing the large scale multi-degree of freedom system. The walking machine, called the Adaptive Suspension Vehicle (ASV; 15x10x5 ft; 7500 lbs) [Waldron and McGhee, 1986] is currently undergoing testing at the Ohio State University. The power system of the vehicle can be divided into three broad categories: leg systems, mechanical transmission system, and the primary power source and energy storage system. Of importance here is the characterization of the complex interactions between the mechanical, hydraulic and computer systems. The modeling issues are many and varied, due to the numerous components involved, and the nonlinear nature of the interactions. They include multi-energy media and a large number of independent variables. The complexity stems not from a lack of understanding of the individual component characteristics but from their interconnections within the system resulting in overall features that are not easily predictable.

A comprehensive nonlinear digital simulation is developed using Advanced Continuous Simulation Language (ACSL) and Fortran for precise performance predictions, interaction studies, parametric studies, and to aid in the design and development process. System integration is found to be a very important issue for the design. Validations of the models is provided by several experiments performed on the vehicle prototype. The simulation has been used to study numerous system characteristics, and also to improve the vehicle performance considerably.

1.0 INTRODUCTION

The ASV power system is schematically shown in Figure 1 with the interconnections between the various subsystems. It shows multiple paths for energy transfer between the subsystems, in contrast to just one for a typical wheeled vehicle. The loads on the leg are primarily to support the vehicle and to propel it forward and the leg structure transmits these loads to the hydraulic actuation systems. The six legs of the ASV have eighteen independent hydraulic actuation systems. The mechanical transmission system interfaces with the primary source of power through a high energy density flywheel. Details pertaining to other system features and control strategies can be found in a number of recent papers [Nair et al., 1989; Waldron et al., 1984 & 1986; Klein et al., 1983; Srinivasan et al., 1984; Orin, 1982].

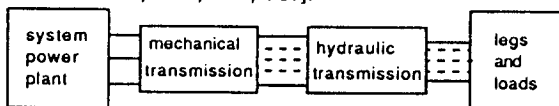


Figure 1 Schematic of the power system of the ASV

Some overall power system modeling issues are listed next while the details are discussed in the subsequent sections. The various modules of the system shown in Figure 1 are combined together with all nonlinearities into a large scale simulation. The

resulting equations are coupled and nonlinear. The leg control algorithms use estimates of the reflected inertia of the leg to determine the control gains. The hydraulic systems actuating the legs are modeled using distributed parameter models which include the nonlinearities due to fluid compressibility and mechanical friction. Since temperature excursions are small, the fluid properties, bulk modulus β and viscosity, were assumed to be constant. Fluid friction effects are comparatively small and are neglected. An energy approach is used to model the interface between the mechanical and hydraulic systems which allows energy to be transferred in both directions with approximately the same efficiency. The mechanical transmission is modeled as a multi-degree of freedom discrete torsional system. Considerations in the modeling of this subsystem are primarily determined by the various interconnections with the other subsystems which include the legs, prime mover and the vehicle accessories. A sixteen degree of freedom discrete model was found to be sufficient to account for all the interconnections. A model for the prime mover, which in this case is an internal combustion engine, is developed and interfaced with the flywheel.

2.0 MODELING

2.1 Leg Dynamics and Loads

Figure 2 shows the coordinates and symbols used in the leg model. The joints are labeled A, B, C, D, E, F and the links are labeled 1, 2, 3, 4. Link 1 is the upper thigh link, link 2 the shank link, link 3 the connecting link, and link 4 the lower thigh link. The foot lift and drive motions are decoupled by this configuration and the foot motion is amplified according to the relations: $z_F = -4z_A$, and $x_F = 5x_C$. Using Lagrange's energy formulation we obtain the dynamic equations of motion for the leg i as follows:

$$F_{axi}(t) = a_{11}(x, z)\ddot{x}(t) + a_{21}(x, z)\ddot{z}(t) + a_{31}(x, z)\dot{x}(t)^2 + a_{41}(x, z)\dot{x}(t)\dot{z}(t) + a_{51}(x, z)\dot{z}(t)^2 + a_{61}(x, z)F_{azi}(t) = a_{12}(x, z)\ddot{x}(t) + a_{22}(x, z)\ddot{z}(t) + a_{32}(x, z)\dot{x}(t)^2 + a_{42}(x, z)\dot{x}(t)\dot{z}(t) + a_{52}(x, z)\dot{z}(t)^2 + a_{62}(x, z) \quad (1)$$

F_{axi} is the force due to the main (x) actuation system at joint C and F_{azi} due to the lift (z) actuation system on joint A. The coefficients $a_{ij}(x, z)$ are nonlinear and lengthy. Figure 3 depicts a typical load profile for one of the legs showing the support phase when the leg is on the ground and the return phase when it is in the air.

2.2 Hydraulic Actuation and Control Strategy

Each leg degree of freedom is actuated independently using a two stage hydraulic system, with a valve-controlled low power control stage and a hydrostatic high power actuation stage. In the hydrostatic stage, each actuator is coupled in a closed circuit with a variable displacement pump. The variable displacement pumps require substantial torques to position their swashplate shafts. For this reason a primary hydraulic stage is used in which the

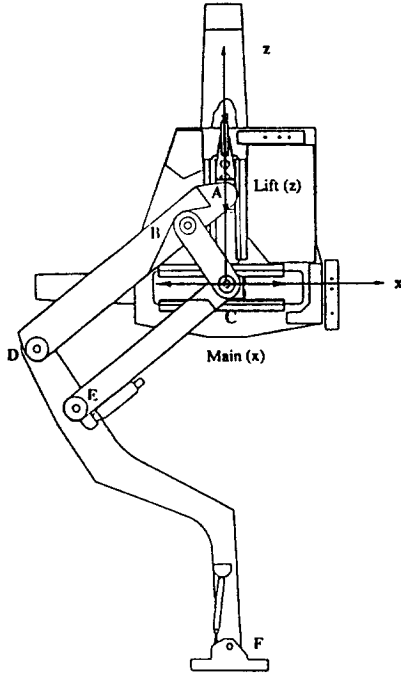


Figure 2 ASV Leg

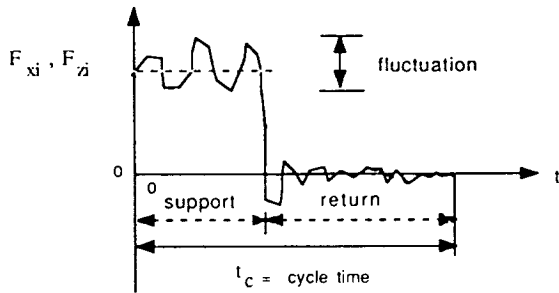


Figure 3 Typical cyclic load profile for the i^{th} leg

swashplate is positioned by a small servovalve controlled rotary actuator. The torques needed to drive the pumps can be estimated if the pressure differences across the actuators are known. The control stage is discussed first followed by the actuation stage and the leg control strategy.

Control Stage : The control stage consists of a servovalve which drives a rotary actuator used to position the swashplate of the variable displacement pump. An accumulator is placed just before the servovalve for supplying the peak flow demands without a large drop in pressure. Analog feedback of the rotary actuator position is used to determine the servovalve input current i_s . The servovalve has been modeled by the following second order transfer function

$$\frac{q_L}{i_s}(s) = \frac{K_{sl}\sqrt{(p_s - p_L)}}{(s^2 / \omega_{ns}^2) + 2\zeta_s(s / \omega_{ns}) + 1} \quad (2)$$

where q_L is the load flow rate, i_s is the input current, $K_{sl}\sqrt{(p_s - p_L)}$ is the servovalve flow gain, p_s is the supply pressure, p_L is the load pressure, ω_{ns} is the natural frequency of the

servovalve and ζ_s is the damping ratio. A discrete model of the connecting lines with equal sized lumps is used in the analysis. The lump size can be estimated using the total line length and the maximum frequency of interest, f_{\max} .

Power Stage : The hydrostatic stage has a variable displacement pump, the swashplate angle of which is set by the control stage, and twin, fixed rod, moving cylinder type linear actuators. The governing equations for the pump, actuator and the load are developed below. The hydrostatic circuits in the x and the z directions are identical. Consider the circuit that powers the drive degree of freedom, in the x direction. The pump is modeled as a pure gain element between swashplate angle ϕ and volume flow rate q as

$$q(t) = K_{pm} \omega_p \phi(t) \quad (3)$$

where K_{pm} is the pump gain and ω_p is the pump speed. Flow balance for the main actuator yields,

$$q(t) = A_x \dot{x}(t) + \left(\frac{V(x)}{\beta}\right) \dot{p}_L(t) + C_l p_L(t) \quad (4)$$

where A_x is the cross sectional area of the actuator, \dot{x} is the actuator rate, $V(x) = V_0 + A_x x$ is the active entrapped volume (the other side is assumed to be at supercharge pressure), V_0 is the volume of the lines, β the bulk modulus, C_l is the total leakage coefficient of the pump and the actuator, and p_L is the pressure difference across the actuator. External leakage is neglected for the pump and the actuator. The subscripts C and A have been dropped from x_C and z_A in the developments that follow, for convenience. Using Equation 3 and 4, we get

$$\dot{p}_L(t) = \left(\frac{\beta}{V(x)}\right) [-A_x \dot{x}(t) - C_l p_L(t) + K_{pm} \omega_p \phi(t)] \quad (5)$$

Finally the force equation is obtained for the x-direction as

$$F_{axi}(t) = A_x p_L(t) - b_l \dot{x}(t) - F_f \quad (6)$$

where b_l is the coefficient of viscous friction in the actuator and F_f is the Coulomb friction in the actuator.

Control Strategy : Linear state feedback with inverse planar feedforward is used to control the legs. Since the leg interacts with the terrain, special cases of this scheme need to be considered for stability purposes. The state variables are position x , velocity \dot{x} and pressure difference p_L . Swashplate angle ϕ is the controlled variable whose desired value ϕ_d is calculated according to the following control law:

$$\phi_d(t) = K_x(x_d(t) - x(t)) + K_v(\dot{x}_d(t) - \dot{x}(t)) + K_p(p_{Ld}(t) - p_L(t)) + \phi_{ff}(t) \quad (7)$$

where K_x , K_v and K_p are the position, velocity and the pressure gains respectively for the x-degree of freedom and ϕ_{ff} is the feedforward term.

2.3 Interface Between Mechanical and Hydraulic Transmissions :

Mechanical energy is transmitted to the legs where it is converted to hydraulic form and is then used to actuate the legs. The model for the interface between the mechanical and the hydraulic transmission systems is shown in Figure 4. In the hydrostatic pump controlled actuation scheme, the swashplate angle ϕ of the variable displacement pump is the controlled variable. The torque T needed to drive the pump is given by the specific pump displacement K_{pm} and the pressure difference Δp across the pump as

$$T(t) = D_p \Delta p(t) + T_f = (K_{pm} \phi(t)) \Delta p(t) + T_f \quad (8)$$

where D_p is the displacement of the pump and T_f is the Coulomb friction in the pump. T_f is estimated experimentally using energy loss data. Since variation of the pump shaft speed is small, viscous

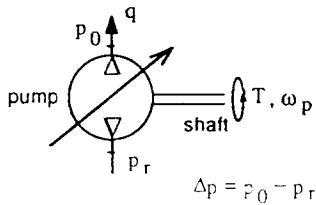


Figure 4 Pump-shaft interface

friction is not considered separately. A negative value of torque T implies that the pump reverts energy back to the transmission system, otherwise it requires energy from it. This torque T is provided by an elaborate mechanical transmission system which interconnects all the eighteen leg actuation pumps in the system.

2.4 Mechanical Transmission Dynamics

The mechanical transmission system is shown schematically in Figure 5. Three quill shafts driven from the flywheel output shaft run along the length of the body of the

flywheel shaft and the quill shafts and between the quill shafts and the pump shafts. Belt stiffness is assumed to be constant and has been determined experimentally by inserting a segment of the belt wound over two pulleys in a tensile testing machine. Transverse belt vibrations have been neglected.

Using a lumped parameter scheme for the shafts, a sixteen degree of freedom torsional model of the transmission system has been developed (Figure 5). The inputs to the model are the engine torque T_e and the pump torques at the six leg locations. The pump torques can be related to the forces on the legs. A general inertia element J_i in the torsional system is depicted in Figure 6 showing the constraint forces acting on it. The equation of motion for the i^{th} element is:

$$\begin{aligned}
 & J_i \ddot{\theta}_i + k_{i,i-1}(\theta_i - \theta_{i-1}) + k_{i,i+1}(\theta_i + \theta_{i+1}) \\
 & + b_{i,i-1}(\dot{\theta}_i - \dot{\theta}_{i-1}) + b_{i,i+1}(\dot{\theta}_i + \dot{\theta}_{i+1}) \\
 & + k_{Bm} r_i (r_i \theta_i - r_x \theta_x) + b_{Bm} r_i (r_i \dot{\theta}_i - r_x \dot{\theta}_x) \\
 & + k_{Bl} r_i (r_i \theta_i - r_y \theta_y) + b_{Bl} r_i (r_i \dot{\theta}_i - r_y \dot{\theta}_y) \\
 & = K_{pm} \omega_p \sum (\phi_i \Delta p_i) - \sum T_{fi} \quad (9)
 \end{aligned}$$

LEFT

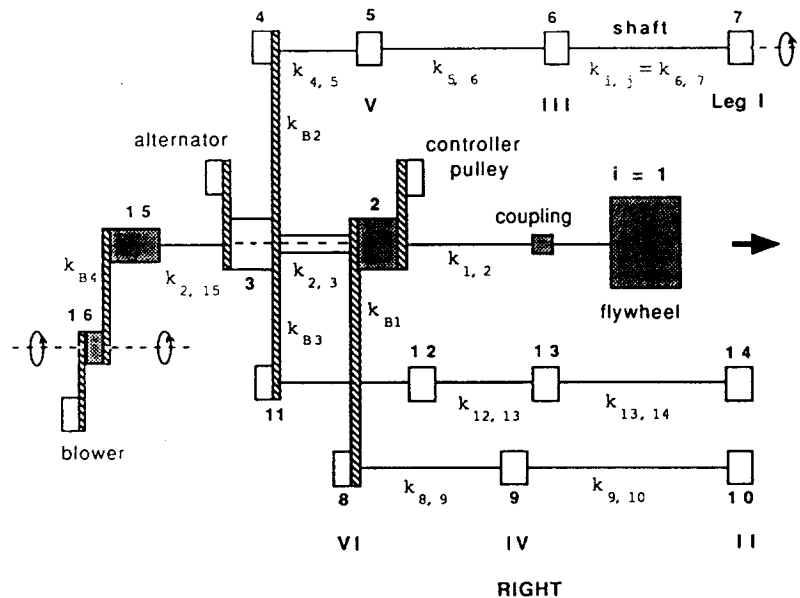


Figure 5 Torsional model of the mechanical transmission

machine. Of these, two run along the top left and right sides of the body frame through the lateral swing bearings at which the legs mount to the body, while the third runs along the bottom of the frame along the center line. The shafts that run along the top power the main and lift pumps of the hydraulic system, while the shaft that runs through the bottom powers the pumps that actuate the lateral degree of freedom of each leg. A belt and pulley arrangement is used to transmit power between the flywheel output shaft and the quill shafts. The coupling between the pulley and the shaft ensures that only torques are transmitted to the quill shaft without any longitudinal or bending force. All six legs are powered by the quill shafts, using independent hydrostatic pump controlled linear actuators as explained earlier.

The shafts in the mechanical transmission system are discretized using the following criterion for the lump length, $l \leq \sqrt{G/\rho} / 10f_{max}$ where f_{max} is the maximum frequency of interest, G is the shear modulus and ρ is the density of the shaft material. Toothed belts are used to transmit power between the

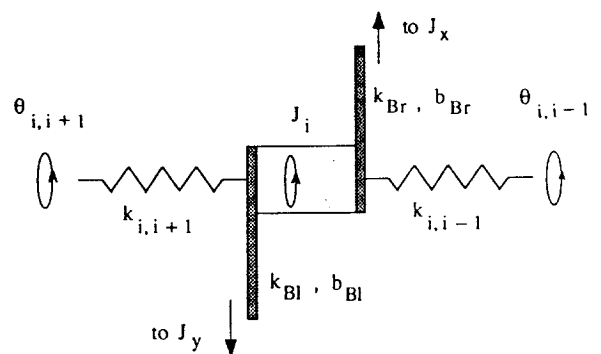


Figure 6 Schematic of a general torsional inertia element in the drive train model

where θ_i is the angular displacement of J_i , $k_{i,j}$ is the torsional stiffness of the shaft segment connecting J_i to J_j , $b_{i,j}$ is the coefficient of viscous damping of the shaft segment, k_{Bm} is the stiffness of the belt m connected to J_i , b_{Bm} is its coefficient of viscous damping, r_i is the diameter of the pulley at station i , r_x is the diameter of the pulley at station x . The terms on the right hand side represent the torques due to the actuation systems described earlier. The equations for the 16 degree of freedom torsional system can be written in matrix form as

$$J\ddot{\theta} + B\dot{\theta} + K\theta = T \quad (10)$$

where $\theta = [\theta_1, \theta_2, \dots, \theta_{16}]^T$ and J , B , and K are the system mass, stiffness and damping matrices, each of dimension 16×16 and T is the force vector (16×1). J is diagonal with entries J_i , $i = 1, 6$. The damping matrix B has the same structure as that of K . The structure of the input force vector T depends on the inputs to the various leg actuation systems and also on the engine and its controller. The terms on the right hand side of Equation 9 form one set of inputs. The first two terms in these relate the pressure in the linear actuators of the actuation system to the torques on the mechanical transmission system. The engine is modeled as a torque source, with the throttle position α as input with the leg systems providing the load torque T_L .

2.5 Overall Model and Inputs

The various modules were appropriately cascaded to get a digital simulation of the entire power system, as shown schematically in Figure 7. The inputs to the simulation include the vehicle velocity v_M , the gait parameters including the duty factor β_d (fraction of the cycle time that the leg is on the ground), the leg stroke R_l , the initial flywheel speed ω_{fw} , the interaction forces between the leg and the ground F_{xi} and F_{zi} determined by the force allocation algorithm [Kumar and Waldron, 1987] and the engine torque T_e . The leg cycle frequency f_c is related to the vehicle

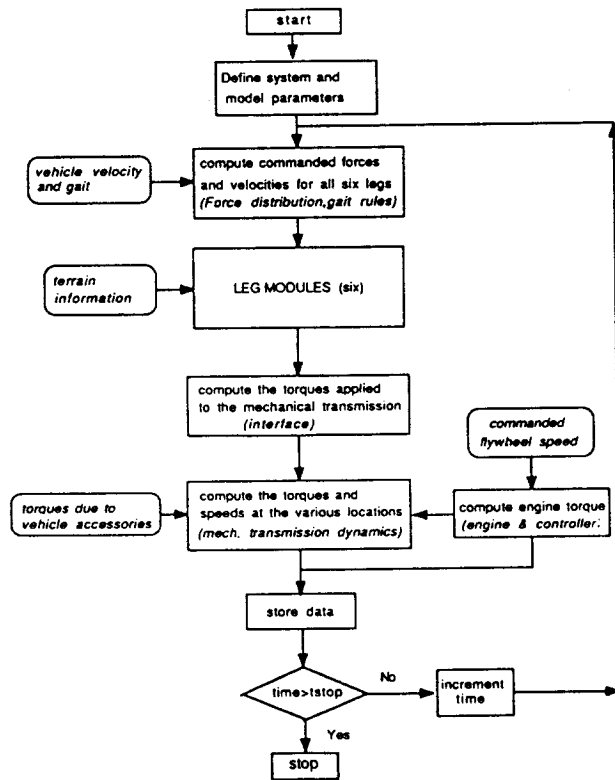


Figure 7 Flow chart of the simulation

velocity v_M as $f_c = v_M \beta_d / R_l$ where β_d is the duty factor for the gait and R_l is the leg stroke.

The simulation modules are written Advanced Continuous Simulation Language (ACSL) and Fortran. The program development and processing of results has been done on the Mechanical Engineering VAX 8550 mainframe computer using PLTPAK plotting routines.

2.6 Test Conditions

The prototype vehicle is designed to operate in six different modes. It can be shown that the loads, and load fluctuations, on the drive train increase in those modes in which fewer legs support the vehicle. For static stability a minimum of three feet need to be on the ground at all times. Surmounting obstacles is another set of maneuvers in which large loads on the drivetrain are expected. The digital model developed here was used to simulate some of the vehicle maneuvers and to study their effect on the power system. Experimental torque data was obtained for two of the maneuvers using a strain gage set-up in order to validate the simulation predictions.

A. STANDING ON SIX LEGS : The vehicle is assumed to be standing still with all of its systems operational. In this maneuver the loads on the drivetrain are due to the upward forces on each leg which are equal, $F_{xi} = 0$ and $F_{zi} = W/6$ for $i = 1, 6$, where W is the weight of the vehicle and F_{xi} and F_{zi} are the foot forces in the main and lift direction for leg i respectively. In the first maneuver, the engine is switched off after spinning the flywheel up to the desired speed. The flywheel spin down rate thus represents the system energy consumption rate, P . In this case, $P = J_{fw} \omega_{fw} \alpha_{fw}$

, where ω_{fw} and α_{fw} are the angular velocity and acceleration of the flywheel respectively. The total power consumption data can thus be recorded experimentally by monitoring the flywheel speed. Energy is consumed to operate all the vehicle systems and to provide for the leakage losses in the lift pumps. The other simulation inputs are constant leg positions and zero leg velocities.

B. TRIPOD GAIT : The Tripod gait is used by the machine in the cruise mode of operation. In this mode three feet are on the ground at any given instant: the front and rear legs of one side and the middle leg of the other side, forming a 'tripod' (either legs 1,4,5 or 2,3,6). The middle legs bear approximately half the weight of the vehicle throughout the contact period. The loads on the front and the rear contact feet vary approximately linearly between a minimum value close to zero and a maximum which approaches half the vehicle weight [Huang and Waldron, 1987]. In one set of simulation runs it is assumed that the vehicle has attained constant velocity and thus $F_{xi} = 0$ for all i . Since the resistance forces opposing forward motion are negligible, this assumption is justified. In the other set of runs, the vehicle is assumed to be walking up a 60% grade at a constant velocity.

The maneuver of obstacle crossing can also be studied using the simulation. In this maneuver, the gait used is a Follow-the-Leader (FTL) gait in which the rear legs step in the footprints of the front ones, the positioning of the latter being controlled by the operator [Song, 1986]. The power consumption in this maneuver is dependent on the speed of operation. Currently this maneuver is performed at slow speeds with low power demands.

3.0 RESULTS

3.1 Leg System

A numerical simulation of the leg system including the leg dynamics compares very well with measured results for the trajectory tracking. The state vector for each actuation system comprises of the displacement and velocity of the actuators and the pressure difference across the actuators: $\{x, \dot{x}, p_{Lx}\}$ and $\{z, \dot{z}, p_{Lz}\}$. The lateral (y) degree of freedom has not been exercised during the tests. Position and velocity transducers and differential pressure transducers are used to measure the signals. The digital control algorithm is implemented using an Intel 86/30 Single Board Computer which interfaces with the operator through a VT101 terminal. Only the transfer phase

trajectory control is studied since in the support phase the legs are used as sources of force with leg motion being passively controlled by the body. Figure 8 shows the profile for the main actuator displacement x_C and the lift actuator displacement z_A for a typical walking cycle. It should be noted that the displacement of the foot is given by $x_F(t) = \gamma_x x_C(t)$ and $z_F = \gamma_z z_A(t)$ where γ_x is the kinematic magnification factor between actuator motion and foot motion for the x-direction and γ_z for the z-direction. The leg is in transfer phase when it traverses from 0 to t_1 seconds and in the support phase for the rest of the cycle. The discrepancy between the predicted and measured values is less than 3% for the displacement time history. The simulation also predicts the pressure and velocity histories well. The experimental results for the flywheel spindown and shaft torque also compared well with simulation predictions.

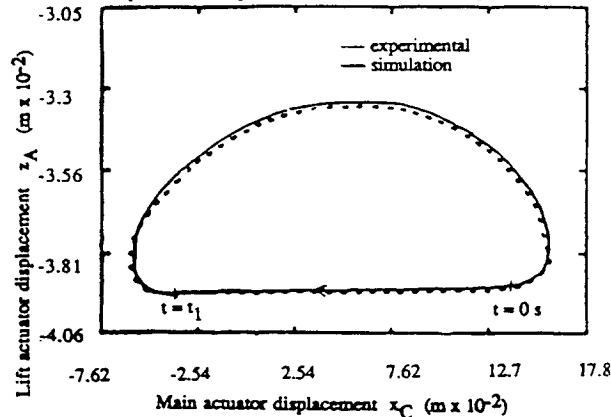


Figure 8 Comparison of simulation and experimental actuator displacement trajectories; $f_c = 0.3$ Hz

3.2 Overall Simulation

The characteristics of the power system variables for a typical vehicle maneuver are presented to illustrate some of the capabilities of the simulation. Of the variables, exceeding 30 in number, some are depicted in Figures 9, 10 and 11 for the following maneuver: vehicle velocity $v_M = 1.8$ m/s (3.6 ft/s); vehicle acceleration $a_M = 0$; terrain gradient $\mu = 0$; leg stroke $R_l = 1.62$ m (5.4 ft); duty factor $\beta_d = 0.5$; leg cycle frequency $f_c = 0.33$ Hz; engine time constant $\tau = 1$ sec; flywheel inertia $J_{fw} = 0.37$ N-m-s² (3.24 lbf-in-s²).

The initial four cycles that show the transient response have been neglected. The frequency of fluctuations is twice the leg cycle frequency. This is due to the fact that there are two alternating support patterns - legs 1,4,5 and legs 2,3,6, over one cycle in tripod gait with $\beta_d = 0.5$. Figure 9(a) shows the engine torque time

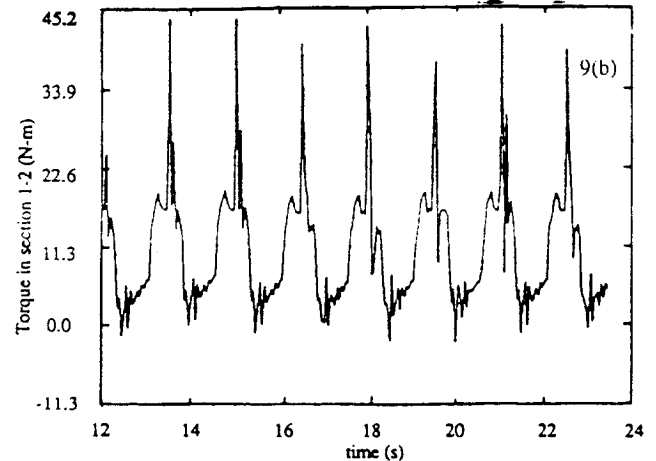
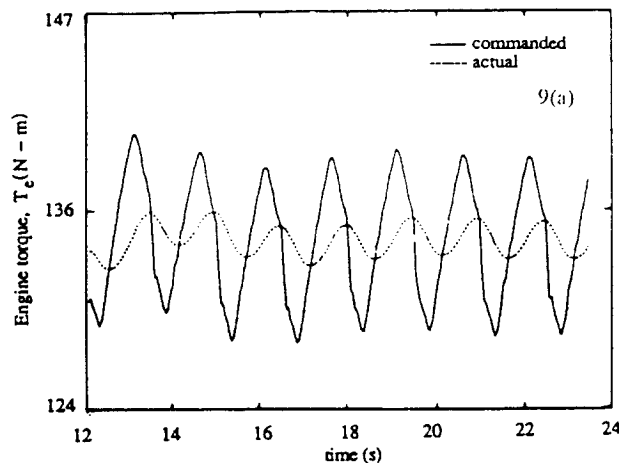


Figure 9 Simulation torque histories

history which depends on the engine time constant τ . Figure 9(b) shows the torque in a representative shaft section 1-2. Figure 10 shows the pressures in the drive and lift actuators for leg 3. The pressure histories show that the system is underdamped during the transfer phase (position and velocity control only), while, in the support phase the damping prevents any overshoot (force or pressure control only). Figure 11 shows a typical parametric study useful for flywheel sizing where the engine torque fluctuation is

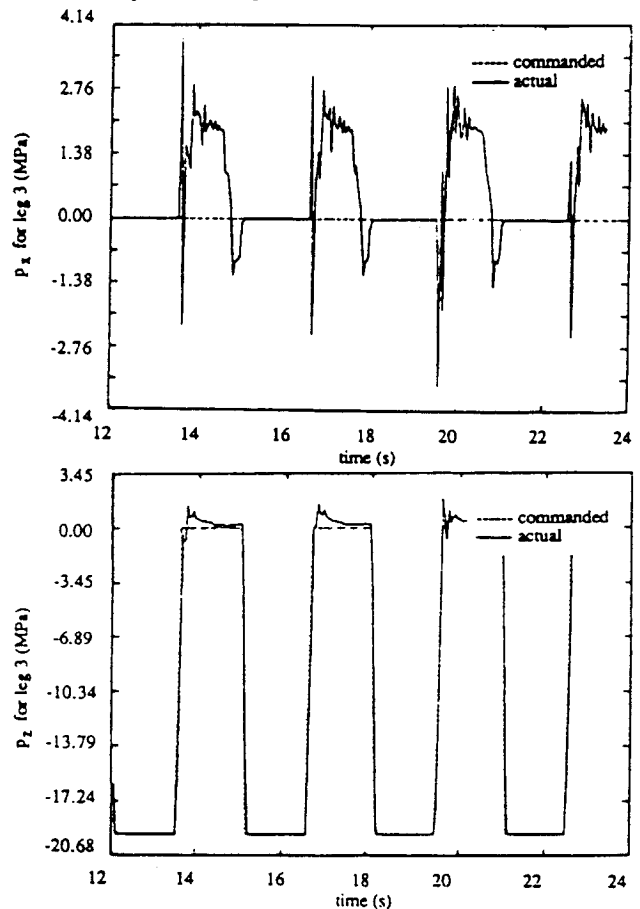


Figure 10 Simulation pressure histories

shown for varying flywheel sizes. These and similar studies are being used performance improvement studies.

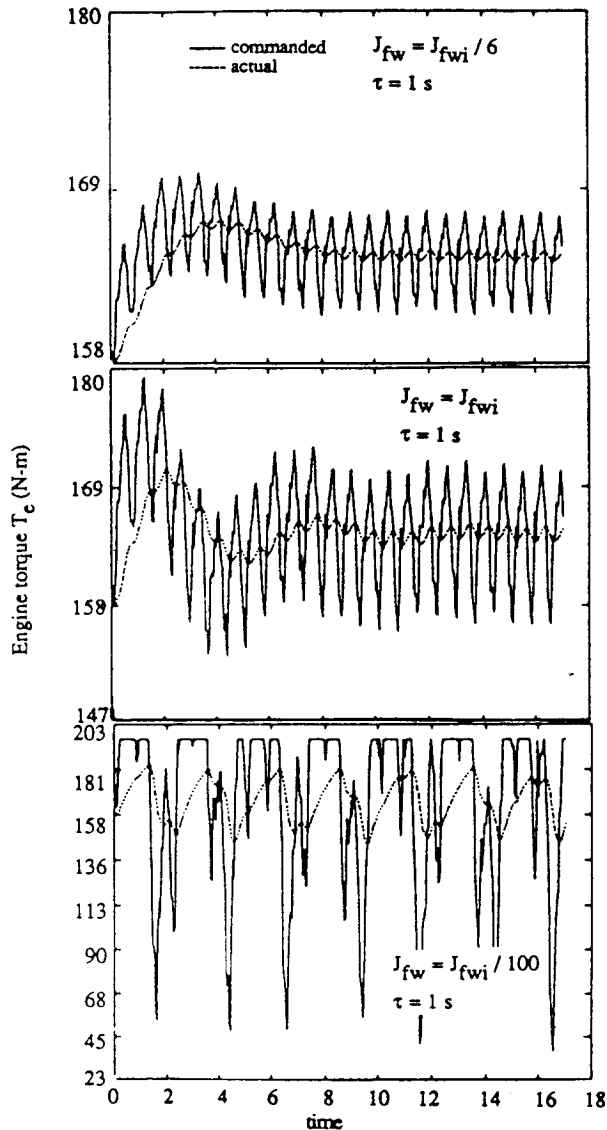


Figure 11 Parametric studies : Effect of flywheel size on engine torque

4.0 DISCUSSION

The different algorithmic modules based on mathematical models of subsystems and components have been successfully integrated to establish a realistic and reliable digital simulation of the entire system including all nonlinearities. Due to the numerous interconnections and nonlinearities, digital simulation was found to be an essential complement to analytical models in system analysis. Using ACSL and Fortran modules reliable simulations having a high degree of accuracy have been developed. The simulation serves as a test bed for leg control algorithm studies, interaction studies, and also for optimization purposes. Optimization of the system would include sizing of the shafts, belts and other system components. The simulation has been developed with a flexible structure so that additional details can be included in any of the modules if necessary. Also, different features of the system can be exercised using

appropriate inputs to study the system characteristics and interaction effects. Many of the models can be extended to study similar robot power and control systems.

5.0 ACKNOWLEDGEMENTS

The reported work formed part of the author's doctoral research at the Ohio State University. The author is indebted to Professors R. Singh and K.J. Waldron for their encouragement and guidance, as well as support from the Defense Advanced Research Projects Agency contract DAAE07-K-R001. The assistance provided by V.J. Vohnout, D. R. Pugh, L. Fisher and others of Adaptive Machine Technologies, Inc. is also appreciated.

6.0 REFERENCES

- [1] Adaptive Machine Technologies, 1987, Personal Communications
- [2] Dworak, J. A., Srinivasan, K., and Waldron, K. J., December 1986, "Digital Control of a Hydraulic Circuit for a Walking Vehicle", *ASME Paper No. 86-WA/DSC-7*, ASME Winter Annual Meeting, Anaheim, California
- [3] Gardner, J. Y., Dworak, J. A., Srinivasan, K., and Waldron, K. J., September 1983, "Design and Testing of a Digitally Controlled Hydraulic Actuation System for a Walking Vehicle Leg Mechanism", *Proceedings of the Eighth Applied Mechanisms Conference*, St. Louis, pp. 2-1 to 2-7
- [4] Huang, M.Z., and Waldron, K. J., 1987, "Relationship between Payload and Speed in Legged Locomotion", *Proceedings of the IEEE International Conference on Robotics and Automation*, Raleigh, NC, Vol.1, pp. 533-538
- [5] Klein, C. A., Olson, K. W., and Pugh, D. R., Summer 1983, "Use of Force and Attitude Sensors for Locomotion of a Legged Vehicle Over Irregular Terrain", *International Journal of Robotics Research*, vol. 1, no.1, MIT Press
- [6] Kumar, V., and Waldron, K. J., 1988, "Force Distribution in Closed Kinematic Chains", *Proceedings of the IEEE International Conference on Robotics and Automation*, Philadelphia, PA, pp. 114-119
- [7] Nair, S., Singh, R., Waldron, K.J., and Vohnout, V.J., June 1989, "Power System of a Multi-Legged Vehicle", to be presented at the *Fourth International Conference on Advanced Robotics*, Columbus, Ohio
- [8] Orin, D., Spring 1982, "Supervisory Control of a Multi-legged Robot", *International Journal of Robotics Research*, vol.1, no.1, MIT Press
- [9] Song, S. M., Waldron, K. J., and Kinzel, G. L., 1985, "Computer-Aided Design of Legs for a Walking Vehicle", *Proceedings of the 8th Oklahoma State University Applied Mechanisms Conference*, St. Louis, Missouri.
- [10] Srinivasan, K., Holloway, M., and Waldron, K. J., August 1984, "Control of a Hydraulically Powered Walking Machine Leg", *Proceedings of the First Fluid Power National Education Seminar*, pp. 115-134
- [11] Waldron, K. J., Vohnout, V. J., Pery, A., McGhee, R.B., Summer 1984, "Configuration Design of the Adaptive Suspension Vehicle", *International Journal of Robotics Research*, 3(2)
- [12] Waldron, K. J., and McGhee, R. B., Dec 1986, "Adaptive Suspension Vehicle", *IEEE Control Systems Magazine*